WATER RESOURCES RESEARCH, VOL. 45, W05409, doi:10.1029/2008WR007233, 2009

Click Here for Full Article

River stage tomography: A new approach for characterizing groundwater basins

Tian-Chyi J. Yeh,[1,2] Jianwei Xiang,[1] Raghavendra M. Suribhatla,[1] Kuo-Chin Hsu,[2] Cheng-Haw Lee,[2] and Jet-Chau Wen[3]

Received 19 June 2008; revised 16 February 2009; accepted 12 March 2009; published 9 May 2009.

[1] Data from tomographic surveys make an inverse problem better posed in comparison to the data from a single excitation source. A tomographic survey provides different coverages and perspectives of subsurface heterogeneity: nonfully redundant information of the subsurface. Fusion of these pieces of information expands and enhances the capability of a conventional survey, provides cross validation of inverse solutions, and constrains inherently ill posed field-scale inverse problems. Basin-scale tomography requires energy sources of great strengths. Spatially and temporally varying natural stimuli are ideal energy sources for this purpose. In this study, we explore the possibility of using river stage variations for basin-scale subsurface tomographic surveys. Specifically, we use numerical models to simulate groundwater level changes in response to temporal and spatial variations of the river stage in a hypothetical groundwater basin. We then exploit the relation between temporal and spatial variations of well hydrographs and river stage to image subsurface heterogeneity of the basin. Results of the numerical exercises are encouraging and provide insights into the proposed river stage tomography. Using naturally recurrent stimuli such as river stage variations for characterizing groundwater basins could be the future of geohydrology. However, it calls for implementation of sensor networks that provide long-term and spatially distributed monitoring of excitation as well as response signals on the land surface and in the subsurface.

Citation: Yeh, T.-C. J., J. Xiang, R. M. Suribhatla, K.-C. Hsu, C.-H. Lee, and J.-C. Wen (2009), River stage tomography: A new approach for characterizing groundwater basins, *Water Resour. Res.*, *45*, W05409, doi:10.1029/2008WR007233.

1. Introduction

[2] Managing groundwater resources in a groundwater basin requires information about hydraulic property distributions, which controls water and contaminant movement and distributions in the basin. With this information, numerical groundwater models are used for simulation, prediction, and scenario analysis, and facilitate long-term management of water resources.

[3] Hydraulic properties of aquifers in a basin (aquifers of tens and hundreds of kilometers) are generally obtained from groundwater model calibration efforts (i.e., inverse modeling of a groundwater flow model with distributed parameters). Many basin-scale model calibrations have not attempted to build detailed heterogeneity into flow models because of the prohibitive cost of detailed sampling over large areas and the computational limits on calibrating multiscale heterogeneity in the model. Regional geologic or hydrologic units are often treated as zones, assumed to be homogeneous with a single effective parameter value [e.g., *Barlebo et al.*, 2004; *Thorne et al.*, 2006].

[4] In these groundwater model calibration efforts, the parameter distribution is often estimated from a steady state or predevelopment head distribution [e.g., *Yeh and Mock*, 1996; *Thorne et al.*, 2006]. Heterogeneous transmissivity fields are estimated by manually adjusting parameter values in model cells or zones to match simulated and observed hydraulic heads. More advanced approaches use automated calibration algorithms (e.g., PEST [*Doherty*, 2007] or UCODE [*Poeter et al.*, 2005]) to minimize the residual between observed and simulated heads [e.g., *Barlebo et al.*, 2004]. Steady state calibrations are limited to estimating transmissivity, and few regional studies attempt to calibrate groundwater flow models using transient head measurements because of the large increase in complexity and computational effort.

[5] Calibrating a basin-scale groundwater model is solving an ill posed problem and results are nonunique because of difficulties in collecting the necessary and sufficient information which makes an inverse problem well posed [*Yeh et al.*, 2007]. For example, sources of excitations in aquifers are rarely fully characterized and frequently only sparse temporal and spatial responses of aquifers are available. As a result, inverse modeling efforts yield aquifer characterization with great uncertainty. Because of this uncertainty, many misleading predictive models of groundwater flow and contaminant migration have been produced.

[1]Department of Hydrology and Water Resources, University of Arizona, Tucson, Arizona, USA.
[2]Department of Resources Engineering, National Cheng Kung University, Tainan, Taiwan.
[3]Department of Environmental and Safety Engineering, Research Center for Soil and Water Resources and Natural Disaster Prevention, National Yunlin University of Science and Technology, Touliu, Taiwan.

Copyright 2009 by the American Geophysical Union.
0043-1397/09/2008WR007233$09.00

The ability to predict flow and solute transport in aquifers have therefore been seriously questioned [*Konikow and Bredehoeft*, 1992; *Bredehoeft*, 2003].

[6] To improve our ability to characterize aquifers, many researchers have recently developed a new aquifer characterization approach: hydraulic tomographic surveys [e.g., *Gottlieb and Dietrich*, 1995; *Vasco et al.*, 2000; *Yeh and Liu*, 2000; *Bohling et al.*, 2002; *Brauchler et al.*, 2003; *Zhu and Yeh*, 2005, 2006]. Hydraulic tomography involves collecting groundwater responses at many locations of an aquifer induced by a sequence of pumping tests at different locations, and then calibrating a heterogeneous groundwater flow model using these observed responses from all the tests. These multiple sets of aquifer tests and corresponding responses provide many constraints for the calibration, since different tests bring forth new information, which validates and/or improves the calibration on the basis of previous tests. As a result, the estimated hydraulic property fields from the calibration become more detailed and less uncertain than those estimated from a single set of data collected from traditional characterization methods.

[7] Hydraulic tomography has been applied successively to small-scale synthetic aquifers [*Yeh and Liu*, 2000; *Zhu and Yeh*, 2005, 2006; *Hao et al.*, 2008], laboratory sandboxes [*Liu et al.*, 2002, 2007; *Illman et al.*, 2007], plot-scale fields [*Vesselinov et al.*, 2001; *Bohling et al.*, 2007; *Straface et al.*, 2007; *Li et al.*, 2007a] and a fractured granite field site [*Illman et al.*, 2009]. In these small-scale studies it is possible to stress the entire domain with each pumping well, providing new information throughout the domain from each pumping event.

[8] Unlike the previous applications of hydraulic tomography, it is not possible to pump a single well to produce a response throughout the basin-scale aquifer unless the pumping rate and test length are unreasonably large. At the basin scale, *Kuhlman et al.* [2008] reformulated hydraulic tomography as an interference problem. The head distribution due to multiple simultaneous pumping wells is observed using a monitoring well network as might be found in a municipal water supply or remedial well field (as proposed by *Yeh and Lee* [2007]). Rather than pump successively from individual wells, *Kuhlman et al.* [2008] cycled through sets of pumping wells. In this way, the regional aquifer is repeatedly stressed to the fullest possible extent using existing wells.

[9] An attractive alternative to multiple simultaneous pumping wells for inducing large hydraulic stresses as simulated by *Kuhlman et al.* [2008] is natural sources of either hydraulic or mechanical stresses that can induce groundwater level responses over the entire basin [see *Yeh et al.*, 2008]. Aquifers are known to respond to such mechanical stresses (see *Kümpel et al.* [1999] or textbook by *Domenico and Schwartz* [1997] for a review) because of naturally occurring atmospheric pressure variations at the surface, periodic solid earth tides, ocean tides and even precipitation at the surface [e.g., *Sophocleous et al.*, 2006; *Desmarais and Rojstaczer*, 2002]. Likewise, recharge from and discharge to surface water bodies such as rivers and lakes induce hydraulic gradients over a multitude of spatial scales ranging from local to regional flow systems (see *Winter* [1999] for an excellent overview).

[10] Numerous studies have been conducted in the past to estimate the hydrogeologic properties of aquifers by interpreting the aquifer response due to naturally occurring mechanical stresses [*DeWiest*, 1965; *Rojstaczer*, 1988; *Rojstaczer and Riley*, 1990; *Hsieh et al.*, 1988; *Davis et al.*, 2000; *Li et al.*, 2007b] as well as hydraulic stresses due to river stage variations [*Duffy et al.*, 1978; *Nevulis et al.*, 1989; *Sophocleous*, 1991; *Barlow et al.*, 2000; *Vazquez-Sune et al.*, 2007]. A comprehensive review of interactions between surface water and groundwater systems (SWGW) at various spatial and temporal scales has been presented by *Sophocleous* [2002]. Past field studies and data analyses have relied on analytical solutions for homogeneous aquifers [e.g., *Moench and Barlow* [2000]; *Kollet and Zlotnik*, 2003].

[11] Very few studies have investigated effects of aquifer heterogeneity on the groundwater fluctuation induced by river stage variations in a groundwater basin. *Sophocleous* [1991] hypothesized that groundwater level rises in the Great Bend Prairie aquifer of Kansas are not only caused by water percolating downward through the vadose zone but also by pressure pulses from stream flooding that propagate in a translatory motion through numerous high-transmissivity and high-hydraulic diffusivity buried channels (paleochannels). These paleochannels cross the Great Bend Prairie aquifer in an approximately west to east direction. Because of the widespread relatively shallow and thin clay layers throughout the Great Bend Prairie, the aquifer behaves essentially as a confined aquifer with low storativity but high transmissivity, thus allowing these pressure pulses to travel rapidly across long distances from the stream source.

[12] In order to validate his hypothesis, two transects of wells (spaced 6 miles apart) oriented north-south and east-west, crossing and alongside some of the paleochannels in the area, were instrumented with water level recording devices. The north-south transect includes eight wells spanning over 68 km (42 miles) of the Great Bend Prairie from Great Bend to Pratt, Kansas. The west-east transect also includes eight wells spanning over 58 km (36 miles) from Larned, Kansas, to east of the Quivira National Wildlife Refuge. Streamflow data from all area streams (including the Arkansas River, Pawnee River, and Rattlesnake Creek) were collected from available stream gauging stations. Precipitation, barometric pressure, and other weather and groundwater recharge–related data were also obtained from existing recharge assessment sites in the area.

[13] These field data sets reveal that observation wells located in between the inferred paleochannels show little or no fluctuations and no correlation with streamflow, even for the wells at short distances (e.g., 1.5 miles) from the river. On the other hand, wells located along the paleochannels at distances ranging from 800 ft to 37 miles away from the river exhibit high water level fluctuations and show good correlation with the streamflow of the stream connected to the observation site by means of the paleochannels. These field data sets also discounted the possibility that the observed groundwater level fluctuations are caused exclusively by significant local differences in precipitation.

[14] In addition, *Sophocleous* [1991] conducted stream-aquifer numerical simulations and demonstrated that the larger the hydraulic diffusivity of the aquifer, the larger the extent of pressure pulse propagation and the faster the

propagation speed. For heterogeneous aquifer systems, zones with identical hydraulic diffusivity values will not result in identical pulse propagation unless they also share the same transmissivity or storativity ratio. The conceptual simulation results indicate that long-distance propagation of stream flood pulses (of the order of tens of kilometers) through the Great Bend aquifer is indeed feasible with plausible stream and aquifer parameters. Moreover, results of the sensitivity analysis indicate that the lower the stream stage, the less its impact on the aquifer. The stream stage is highly sensitive to the Manning coefficient and channel slope. More recently, *Rotting et al.* [2006] conducted stream stage flooding tests in a heterogeneous aquifer-river system and estimated transmissivities, storativities and leakage parameters by coupling stream stage measurements with pumping tests.

[15] Linking the concept of hydraulic tomography with the long-recognized relation between river stages and groundwater level as well as evidence of heterogeneity on flood pulse propagation in aquifers as observed by *Sophocleous* [1991], *Yeh et al.* [2004] and *Xiang and Yeh* [2005] proposed and explored the possibility of the river stage tomography. That is, as the river stage perturbation (e.g., a flood wave or discharge from a dam) migrates to one location along the river, it produces a pressure head response in various parts of the aquifer. These responses in essence constitute a snapshot of the heterogeneity of the aquifer with a hydraulic excitation source at the location of the disturbance. As the flood wave continuously migrates downstream and aquifer responses at various times are collected, we thereby have a large number of snapshots of the aquifer heterogeneity with sources at different locations. These snapshots provide us with the view of the aquifer heterogeneity at different angles and perspectives. Synthesizing these different views should lead to a better characterization of the aquifer heterogeneity than using one snapshot.

[16] In this study, we develop a numerical model to simulate temporal and spatial responses of the aquifer caused by migration of a streamflow perturbation along a river in a synthetic groundwater basin. A stochastic inverse methodology is also adopted that exploits these responses to estimate aquifer properties in the basin. We then conduct numerical experiments to test the river stage tomography concept for delineation of aquifer heterogeneity. Toward the end, we discuss possibilities and difficulties associated with the concept when it is applied to real world scenarios.

2. Flow Model for the SWGW System

[17] Generally, stream and groundwater processes as well as their interactions are complex at various scales: the finer the scale is, the more complex these processes are. To include all processes and their complexities at various scales may be possible but is beyond the scope of this study. The objective of the study here is exploration of the concept of basin-scale aquifer characterization using naturally recurrent events as a basin-scale hydraulic tomographic survey. Specifically, the focus of the study is the basin-wide groundwater level responses to river stage fluctuations in the presence of basin-scale aquifer heterogeneity. Different from simulation conducted by *Sophocleous* [1991], we aim to demonstrate here the possibility of using stream stage variations to delineate the heterogeneity of groundwater basins. To accomplish the objective without loss of realism, a simplified river-groundwater basin system developed by *Glover* [1988], similar to the USGS model [*Trescott et al.*, 1976] used by *Sophocleous* [1991], is considered in this study, which consists of a two-dimensional, heterogeneous semiconfined aquifer and a stream. The stream is simplified as a line source and serves to define the temporal and spatial excitation to the basin aquifer. Groundwater flow in the aquifer is represented by a two-dimensional, depth-averaged equation:

$$S(x,y)\frac{\partial\phi(x,y,t)}{\partial t} - \nabla.(T(x,y)\nabla\phi(x,y,t)) = q(x,y,t) \quad (1)$$

where S denotes the storage coefficient, ϕ is the hydraulic head [L], t is time [T], T represents the transmissivity [L^2/T], and q [L/T] is strength of the line source representing recharge from the stream. The boundary conditions for the aquifer are that of prescribed head and flux:

$$\phi|_{\Gamma 1} = f_1(t) \quad \text{and} \quad T\nabla\phi\cdot n|_{\Gamma 2} = f_2(t) \quad (2)$$

and the initial condition is

$$\phi|(x,y,0) = \phi_0(x,y,0) \quad (3)$$

In our analysis, streamflow in the river is modeled using the kinematic equation for a one-dimensional open-channel flow:

$$\frac{\partial d(l,t)}{\partial t} + \frac{\partial[u(l,t)d(l,t)]}{\partial l} = q_r(l,t) \quad (4)$$

where $d(l,t)$ is the river stage (the depth of the water in the river); l is taken along the length of the river; q_r is the recharge per unit area from the stream to the aquifer, defined in terms of the properties of the streambed and the depth in the stream as

$$\begin{aligned} q_r(l,t) &= \frac{K}{c}d(l,t) \\ Q_r(l,t) &= B\int_l^{l+\Delta l} q_r dl \end{aligned} \quad (5)$$

where K [L/T] is the hydraulic conductivity of the streambed and c [L] is its thickness, B [L] is the width of the stream, and Q_r [L^3/T] is the net rate of recharge over a segment of length Δl.

[18] Note that in this idealized representation of the recharge from the stream as a line source, the recharge depends only on the depth of the stream stage and is assumed to be gravity driven below the stream. This assumption follows from the observation that, for streams that have a large width to depth ratio, the bank storage effects are neglected and the leakage predominantly percolates vertically downward into the aquifer [*Chen and Chen*, 2003]. Additionally, the width of the river is much smaller than the scale of heterogeneity considered in this study so that the local-scale interactions between the river and aquifer may be ignored. Also, storage effects of the medium between the stream and the aquifer have been neglected in our SWGW model. This assumption stems from the findings of numerical simulations by *Zlotnik and Huang* [1999] that neglecting storage effects of the vadose

zone underneath the stream leads to errors that are extremely small in magnitude and can be considered practically irrelevant.

[19] The velocity, u, of the river flow is assumed to be governed by

$$u(l,t) = \frac{1.49}{n} S_0^{\frac{1}{2}} d(l,t)^{\frac{2}{3}} \tag{6}$$

where n is the Manning roughness coefficient, d is the river stage (depth of the river), and S_0 denotes the river channel slope. The river slope and the Manning roughness coefficient are assumed to be constant along the river length. The boundary and initial conditions associated with equation (4) are

$$d|_{l=0} = d_1(0,t) \quad \text{and} \quad d|_{t=0} = d_0(l,0) \tag{7}$$

respectively, and d_1 (0, t) represents the input hydrograph to the river at l = 0. This completes the description of the forward problem for determining head distributions in the aquifer induced by stream stage variations. The groundwater flow equation, kinematic equation, boundary conditions and initial conditions (i.e., equations (1) through equations (7)) are implemented using a finite element approach (VSAFT2, available at www.hwr.arizona.edu/yeh).

3. Inverse Methodology

[20] In river stage tomography, the unknown parameters to be estimated are the spatial distributions of T and S values in the basin-scale aquifer. To conduct this inverse modeling effort, we use a simultaneous successive linear stochastic estimator (SimSLE) developed by *Xiang et al.* [2009]. The SimSLE is an inverse algorithm based on the sequential successive linear estimator (SSLE) developed by *Zhu and Yeh* [2005, 2006] for sequentially synthesizing the aquifer head response due to discrete pumping events during a hydraulic tomography experiment. Instead of incorporating the aquifer's hydraulic head responses from discrete sources sequentially into the estimation as is done in SSLE, the SimSLE method includes all observed groundwater level changes due to migration of river disturbances to different locations simultaneously to estimate T and S of the aquifer.

[21] In the SimSLE approach, the natural logs of T and S values are treated as stochastic processes (i.e., $\ln T = Y + y$ with unconditional mean Y and perturbation y and $\ln S = \Sigma + \sigma$, with the unconditional mean Σ and perturbation σ). Similarly, the hydraulic head is expressed as sum of its mean and perturbation, i.e., $\phi = H + h$. SimSLE then seeks parameters T_c, S_c and H_c (i.e., the conditional effective transmissivity, storage and hydraulic head, respectively) which reflect effects of inclusion of secondary data and direct measurements of T and S. As a result, the simulated head field using these T_c and S_c fields honors head measurements at sample locations and describes conditional "mean" responses of the aquifer to the changes in the river stage following a known input hydrograph and, in turn, recharges the aquifer. The secondary data we use in this study are the head measurements ϕ^* (x, y, t) observed at wells in the aquifer at various times. In addition, this approach implicitly assumes that the river stages along the river reaches are well characterized in time and space along with parameters governing flow in the river. More specifically, this information drives the conditioning process for estimation of the T and S fields.

[22] With given unconditional mean and spatial covariance functions of T and S (i.e., the prior joint probability density is known and is assumed to be multi-Gaussian here), the SimSLE starts with cokriging (a stochastic linear estimator) to estimate the conditional expected value of the property conditioned on f^* ($\mathbf{x}_i$) and h^* (k, $\mathbf{x}_j$, t_l). The term f^* ($\mathbf{x}_i$) represents the perturbation of log hydraulic property, either T or S measured at the ith location, and i = 1,... n_f, where n_f is the total number of f measurements. The term h^* (k, $\mathbf{x}_j$, t_l) denotes the observed groundwater level perturbation at location $\mathbf{x}_j$ at time t_l when the river disturbance has reached a location k. It must be noted here that h^* (k, $\mathbf{x}_j$, t_l) represents the head due to the line source extending in space (and temporally varying) from $k = 0$ to wherever the river disturbance location is at time t_l and not just due to the point source corresponding to the position of river disturbance. The linear estimator is

$$\hat{f}^{(1)}(\mathbf{x}_0) = \sum_{i=1}^{n_f} \lambda_{0i} f^*(\mathbf{x}_i) + \sum_{k=1}^{n_p} \sum_{j=1}^{n_h(k)} \sum_{l=1}^{n_t(k,j)} \mu_{0kjl} h^*(k, \mathbf{x}_j, t_l) \tag{8}$$

where $\hat{f}^{(1)}$ ($\mathbf{x}_0$) is the cokriged f value at location $\mathbf{x}_0$; n_p is the total number of data sets (each corresponding to a specific location of the river disturbance); $n_h(k)$ is the total number of observation wells for the kth data set; $n_t(k, j)$ is the total number of head measurements in time at the jth observation well in the kth data set. The cokriging weight (λ_{0i}) represents contribution of measurement f^* at the ith location to the estimate at location $\mathbf{x}_0$. The contribution to the estimate from the observed head $h^*(k, \mathbf{x}_j, t_l)$ is denoted by μ_{0kjl}. These weights are obtained by solving the cokriging system of equations [see *Xiang et al.*, 2009].

[23] After obtaining the new estimate for all the elements using cokriging, the conditional covariance of f, ε_{ff}, is then determined by

$$\varepsilon_{ff}^{(1)}(\mathbf{x}_m, \mathbf{x}_n) = R_{ff}(\mathbf{x}_m, \mathbf{x}_n) - \sum_{k=1}^{N_f} \lambda_{mk} R_{ff}(\mathbf{x}_k, \mathbf{x}_n) - \sum_{k=1}^{n_p} \sum_{j=1}^{n_h(k)} \sum_{l=1}^{n_t(k,j)} \mu_{mkjl} R_{hf}\left((k, \mathbf{x}_j, t_l), \mathbf{x}_n\right) \tag{9}$$

where m and $n = 1, \ldots n_e$. The unconditional covariance of the parameter is denoted by R_{ff} and cross covariance between h and f by R_{hf}. The conditional covariance reflects the effect of data on the reduction of uncertainty in the estimated parameter field. Subsequently, the estimated log property fields are converted to the arithmetic scale and then used to solve equation (1) for the conditional effective head fields, $h^{(1)}$ (k, $\mathbf{x}_j$, t_n).

[24] Following cokriging, a linear estimator of the following form:

$$\hat{f}^{(r+1)}(\mathbf{x}_0) = \hat{f}^{(r)}(\mathbf{x}_0) + \sum_{k=1}^{n_p} \sum_{j=1}^{n_h(k)} \sum_{n=1}^{n_t(k,j)} \omega_{0kjn}^{(r)} \cdot \left[h^*(k, \mathbf{x}_j, t_n) - h^{(r)}(k, \mathbf{x}_j, t_n)\right] \tag{10}$$

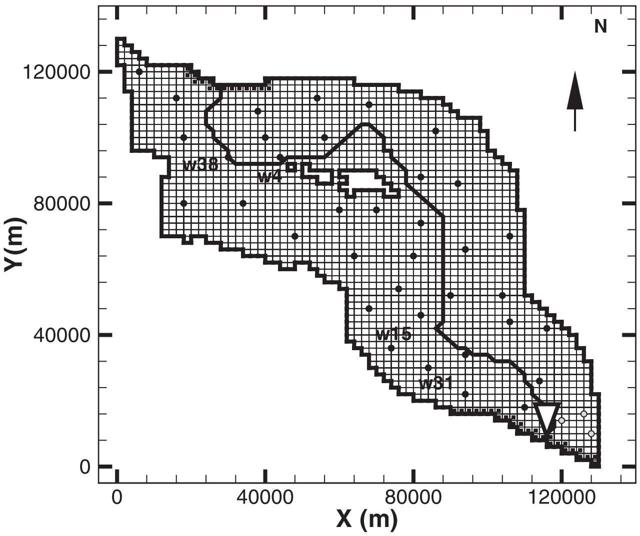

Figure 1. Plan view of the synthetic groundwater basin showing geometry of the river and the aquifer. Dark circles represent locations of the observation wells, and dark squares represent constant head boundaries. The three light circles had low SNR values and were discarded from inverse modeling.

is used to improve the estimate for iteration $r > 1$, where $\omega_{0kjn}^{(r)}$ is the weight term, representing the contribution of the difference between the observed and simulated conditional heads (i.e., h^* (k, $\mathbf{x}_j$, t_n) and $h^{(r)}$ (k, $\mathbf{x}_j$, t_n), respectively) at iteration r at location $\mathbf{x}_j$ of the kth data set at time t_n to the estimate at location $\mathbf{x}_0$. The weights are determined by solving the following system of equations:

$$\sum_{k=1}^{n_p}\sum_{j=1}^{n_h(k)}\sum_{l=1}^{n_t(k,j)}\omega_{0kjl}^{(r)}\left[\varepsilon_{hh}^{(r)}\left((p,\mathbf{x}_m,t_q),(k,\mathbf{x}_j,t_l)\right)+\Theta^{(r)}\delta_{kjl}\right] = \varepsilon_{hf}^{(r)}\left((p,\mathbf{x}_m,t_q),\mathbf{x}_0\right) \tag{11}$$

where $p = 1,\ldots n_p$, $m = 1,\ldots n_h$ and $q = 1,\ldots n_t$. The terms $\varepsilon_{hh}^{(r)}$ and $\varepsilon_{fh}^{(r)}$ are the conditional covariance and the conditional cross covariance at iteration (r), which are evaluated using a first-order approximation based on the conditional covariance of f (i.e., $\varepsilon_{ff}^{(r)}$ which is obtained from equation (9) for the first iteration). A dynamic stabilizer, $\Theta^{(r)}$, is added to the diagonal elements of $\varepsilon_{hh}^{(r)}$ (δ_{kjl} is the Dirac delta, equal to 1 when $k = j = l$ and 0 otherwise) to stabilize the solution to equation (11). The dynamic stabilizer at iteration, r, is the maximum value of the diagonal elements of $\varepsilon_{hh}^{(r)}$ at that iteration times a user-specified multiplier [see *Yeh et al.*, 1996]. After completion of the estimation using equation (10) for all elements in the domain, the conditional covariance of f is updated subsequently as given below:

$$\varepsilon_{ff}^{(r+1)}(\mathbf{x}_m,\mathbf{x}_n)=\varepsilon_{ff}^{(r)}(\mathbf{x}_m,\mathbf{x}_n)-\sum_{k=1}^{n_p}\sum_{j=1}^{n_h(k)}\sum_{l=1}^{n_t(k,j)}\omega_{mkjl}\varepsilon_{hf}^{(r)}\left((k,\mathbf{x}_j,t_l),\mathbf{x}_n\right) \tag{12}$$

where n and $m = 1,\ldots n_e$. Iteration between equations (10), (11), and (12) continues until some convergence criterion is met (see *Xiang et al.* [2009] for details).

[25] Observed well hydrographs often contain noise (i.e., signals caused by processes omitted by the model, including measurement errors, evapotranspiration, regional flow, precipitation, groundwater withdrawal and/or recharge, barometric variation, and many other natural phenomena) in addition to effects of heterogeneity. Such unresolved noises or unaccounted signals can lead to divergence of inverse solutions (i.e., unrealistic estimates). As a consequence, an important issue is what level of observed heads should be used to extract the effect of heterogeneity.

[26] Stabilization of mean square error of the simulated head based on the estimate of the property during iteration provides a way to address this issue [*Xiang et al.*, 2009]. That is,

$$L2_{cond}(r)=\frac{1}{N}\sum_{i=1}^{N}\left(h_i^*-\hat{h}_i^{(r)}\right)^2 \tag{13}$$

where h^*_i and $\hat{h}_i^{(r)}$ are observed and simulated heads, respectively; i is the index denoting the observation in a given time and location from a river stage data set; N is the total number of head observations from all the data sets. Hereafter, we will refer to equation (13) as the conditional L2 norm.

4. Numerical Simulations

4.1. Description of the Synthetic River-Aquifer System

[27] The synthetic groundwater basin considered in this test case consists of a semiconfined aquifer in a river basin deposit bounded by mountains (see Figure 1). The basin is oriented approximately north-south and is 130 km long (north to south) and 130 km wide (east to west). Flow in the 196 km long river enters the basin at the northern end and exits at the southern end as shown in Figure 1. Mountains on either side of the basin act as impermeable boundaries, while the boundary segments near the entry and exit points of the river are constant head boundaries. Notice that in the middle of the basin, there are two impermeable regions, representing outcrops of bedrocks. The synthetic basin was created to mimic the prominent basin topographic features of the Hanford site, Washington [*Thorne et al.*, 2006]. It must be noted here that the model considered in this synthetic test case does not represent the documented geologic and stratigraphic features of Hanford site and this study is not aimed at investigating groundwater flow and aquifer characteristics at the Hanford site.

[28] Model domain for the aquifer is discretized into 1935 square elements, each of a uniform size of 2 km × 2 km. The river is superimposed on the aquifer grid and discretized into lengthwise segments accordingly. Figure 1 shows the cell layout of the modeling domain and the relative locations for the river and the associated flow boundaries. Values of T and S for all the elements in the synthetic aquifer are shown in Figures 2a and 2b, respectively. They were obtained using a stochastic random field generator [*Gutjahr*, 1989] and follow multi-Gaussian probability densities with an exponential covariance function. Mean and variance for the ln$T$ field are 1.06 (the unit of T is m^2/s) and 1.0, respectively and mean and variance of ln$S$ are −13.8 and 0.1, respectively. Correlation lengths are the same for ln T

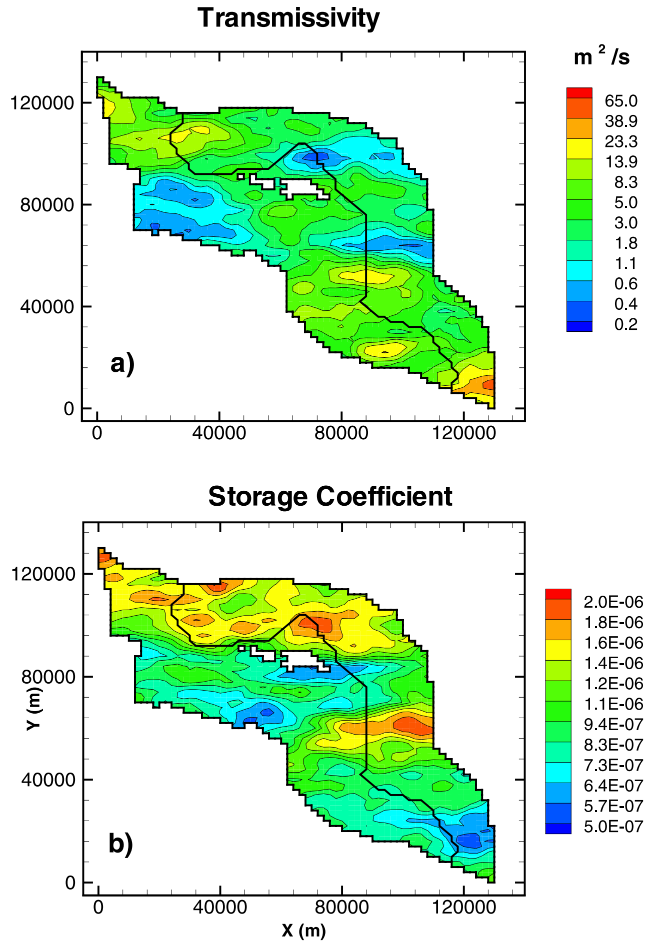

Figure 2. Spatial distributions of true (a) transmissivity and (b) storage coefficient in the synthetic domain.

and ln S fields: 26 km in west to east direction, and 8 km in north to south direction.

[29] Flow in the river and recharge to the aquifer are simulated using channel slope $S_0 = 5 \times 10^{-5}$, the Manning roughness coefficient n = 0.04 (some typical value by *Henderson* [1989]), river width B = 650 m that is constant along the entire length of the river, and a river bed leakage coefficient in equation (5) given as $\frac{K}{c} = 10^{-7}\ s^{-1}$.

4.2. Forward Flow Simulation

[30] Prior to simulating the river disturbance event, the groundwater flow model was run with a constant river flow 4000 m^3/s until the head distribution in the aquifer reached a steady state subjected to the given boundary conditions. This preevent steady state condition serves as the initial groundwater head condition for calculating head changes in the aquifer induced by the flood event.

[31] In order to simulate the river disturbance, a delta shaped stream hydrograph is applied at the upstream point (northern end) of the river at t = 0 s, representing a controlled dam discharge. This stream hydrograph has the following characteristics: inflow to the river during the dam discharge increases linearly from 4000 m^3/s to 13000 m^3/s in 4500 s and decreases to 4000 m^3/s at t = 9000 s (see Figure 3). These flow characteristics are consistent with data reported in by *Kimbrough et al.* [2006] (see "Water Data Report WA-05-1: Klickitat and White Salmon River Basins and the Columbia River from Kennewick to Bonneville Dam," http://pubs.usgs.gov/wdr/2005/wdr-wa-05-1/pdf/wa00103ADR2005_Figure66.pdf). Equations (4) and (6) were solved together using a specified time step for the spatial and temporal distributions of the river stage, $d(l, t)$. Subsequently, recharge to the groundwater system was evaluated using equation (5) at that time step. This net rate of recharge at this time step over a segment of length Δl in equation (5) was then equally distributed to the two nodes of the element of the groundwater flow model (equation (1)) as recharge at the node. Subsequently, equation (1), with the specified recharge per unit area, q (x,y,t), initial and boundary conditions, was then solved for the hydraulic head distribution in the aquifer. The total simulation time is 192,000 s (2.22 days) with a uniform time step of 1,500 s each.

4.3. Aquifer Response to Flood

[32] To conduct the inverse modeling experiment, 39 observation wells were used to record river-induced head changes in the synthetic aquifer. The observation wells were deliberately placed at various distances away from the river (solid circles in Figure 1) to cover the entire aquifer basin. Contour plots of changes in hydraulic head distributions in the aquifer caused by the propagation of the river disturbance at three selected times (namely 30,000, 60,000, and 90,000 s) which correspond to three different locations of the river disturbance are presented in Figures 4a, 4b, and 4c. Figure 4 shows that groundwater wells that are located downstream respond even before the disturbance reaches a location in the river closest to these wells. Figure 5 shows noisy hydrographs recorded at some selected wells (i.e., W4, W38, W15, and W31 in Figure 1) in the aquifer and corresponding denoised hydrographs. As expected, observation wells closest to the river in the lateral direction (i.e., W4, W38) respond faster than those located further away from the river (i.e., W15, W31) as indicated by the arrival time of the peak. Furthermore, irregular shapes of these well hydrographs reflect convolution effects of propagation of

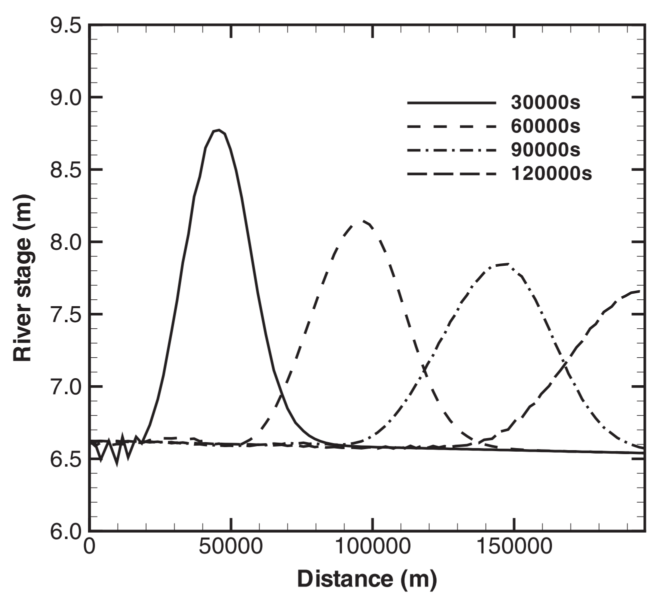

Figure 3. Propagation of the flood wave in the river.

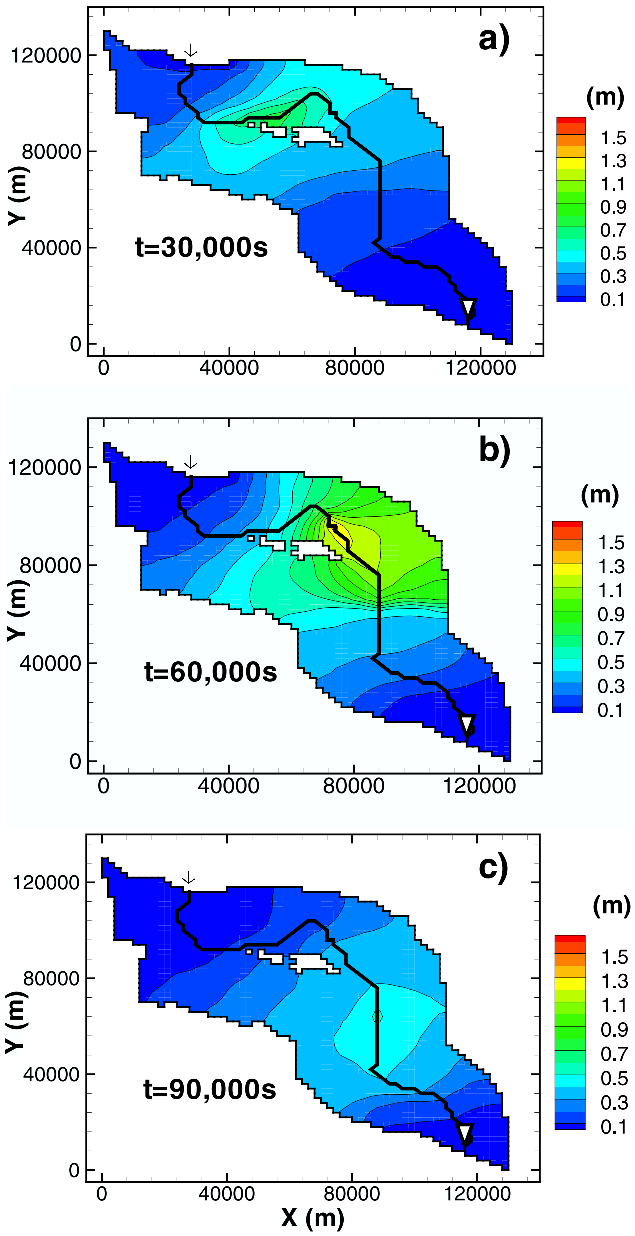

Figure 4. Contour plots of change in heads in the aquifer at three selected simulation times.

the river disturbance as well as the effect of aquifer heterogeneity. The hydraulic behavior induced by propagation of the disturbance are analogous to that induced by a series of groundwater recharge wells distributed along the stream, each of which injects water in to the aquifer at rates varying with time and location according to the streamflow hydrograph. Therefore, measurements of the river stage in essence yield knowledge of the temporal and spatial variable recharge rates that induce the pressure disturbance throughout the aquifer.

4.4. Accounting for Measurement Errors

[33] Observed well hydrographs often contain noise (i.e., signals unaccounted for by the groundwater model) in addition to effects of heterogeneity. Effects of the noise therefore should be considered in the interpretation of the river stage tomography data. For the synthetic test case considered here, white noises with a standard deviation of 0.02 m was superimposed onto the simulated hydrographs. Subsequently, the signal-to-noise ratio (SNR), defined as the ratio of observed drawdown to standard deviation (known) of the noise, is computed for all the observations to assess quality of the well hydrographs. Three wells located in the southeast portion of the domain (shown as light circles in Figure 1) were found to be of poor quality because of their small SNR (<1) and are discarded from the inversion procedure. To eliminate noise in the remaining hydrographs, a wavelet denoising method [*Mallat*, 1999] is used in this study. A detailed procedure for wavelet-based denoising is presented at http://www.mathworks.com.

[34] In this study, we employ the Daubechies-6 wavelet functions and a hard-thresholding method [*Mallat*, 1999] (threshold value = 4) for the wavelet coefficients to denoise the corrupted hydrographs. It is worth mentioning here that the threshold value for wavelet coefficients determines the extent to which the perturbations due to aquifer heterogeneity in a well hydrograph are preserved and not eliminated in the denoising procedure (i.e., the thresholding procedure sufficiently removes noisy components in the signal, but may also "over smooth" the signal). Effectiveness of the wavelet denoising procedure to remove noise from hydrographs at some selected observation wells is demonstrated in Figure 5.

4.5. Performance Assessment

[35] Performance of river stage tomography and SimSLE for the synthetic case was evaluated using the standard correlation measure between the true and the estimated values. A high correlation implies that the two fields are similar in pattern, even though the mean value of the two fields may be quite different. Thereby, in addition to the correlation, mean absolute error (L1 norm) and mean square error (L2 norm) of the estimated field are evaluated.

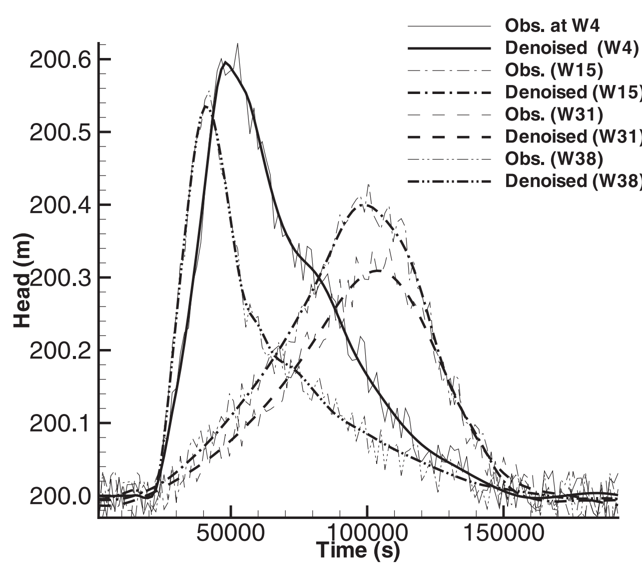

Figure 5. Observed noisy well hydrographs and their denoised counterparts at four selected locations in the aquifer.

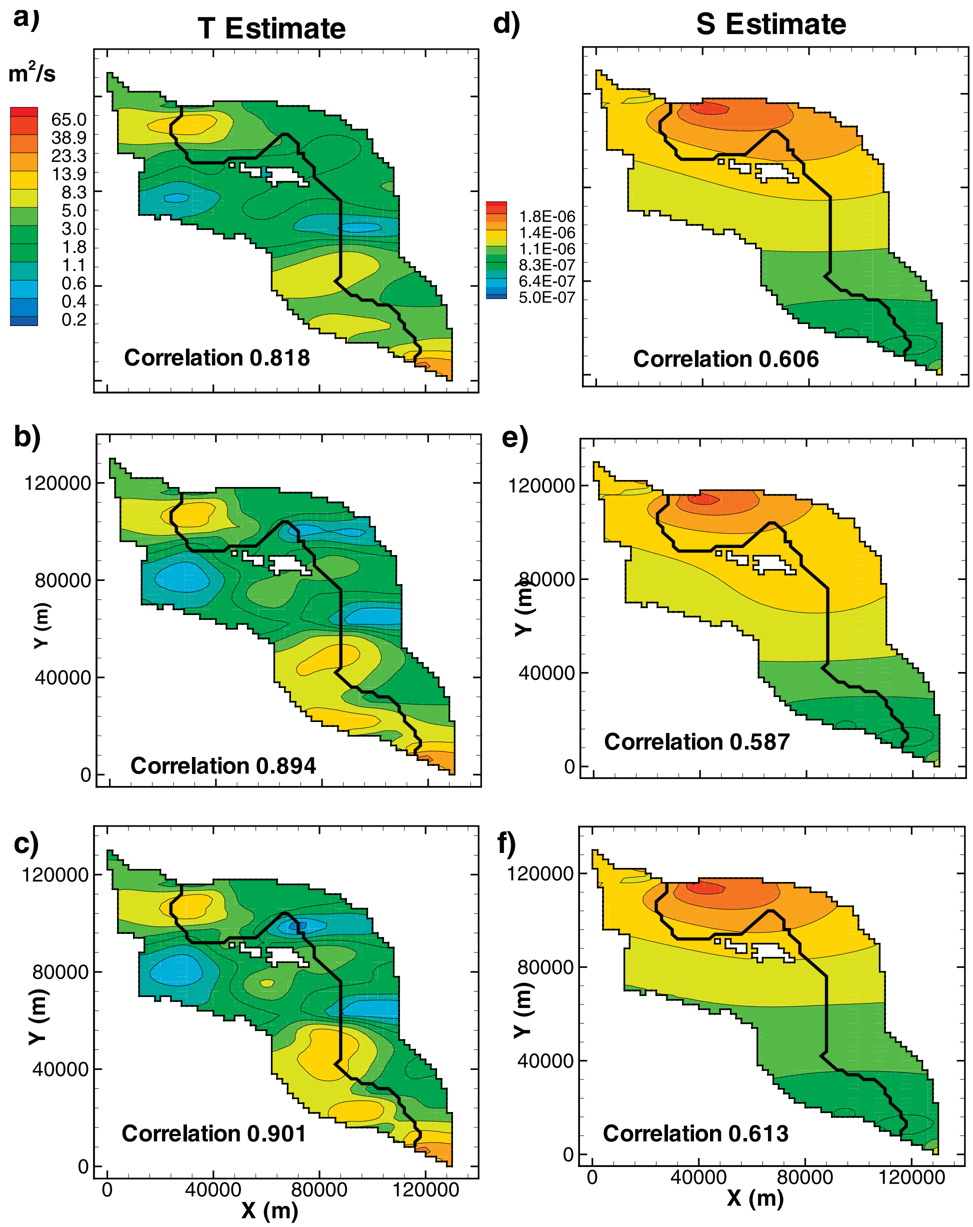

Figure 6. Transmissivity estimates for (a, b, c) cases 1, 2, and 3 and (d, e, f) the corresponding storage estimates.

[36] Besides the correlation analysis as well as the L1 and L2 norms, the similarity between the true and estimated hydraulic property fields was also evaluated with a fuzzy similarity comparison method, which has been applied to the task of comparing spatial patterns [e.g., *Hagen*, 2003]. Details of the fuzzy similarity analysis are also described by *Xiang et al.* [2009].

4.6. Setup and Results of Tomographic Inversion

[37] After denoising the hydrographs, the inversion process is initiated with initial values for the mean, variance and correlation scales of the estimated parameters. For the synthetic case study, these initial values for the structural parameters were set equal to their true mean values. Note that *Yeh and Liu* [2000] and applications of SLE by others [e.g., *Liu et al.*, 2007a] have shown that parameter estimates obtained using the SLE algorithm with sufficient number of secondary data sets are insensitive to the prior information about structural parameters as long as the principal directions of the statistical anisotropy are not significantly different from their true directions.

[38] Additionally, values of T and S are assumed to be known at locations of constant head boundaries (Figure 1) to meet the necessary and sufficient conditions that can make the inverse problem better posed [see *Yeh et al.*, 2007]. Finally, denoised head changes corresponding to four different times at 36 observation wells were used to estimate the spatial distribution of T and S in the basin. Specifically, the first set of estimates (case 1) was based on head changes observed from all wells at time 30,000 s (see Figure 4a), and the estimated T and S are illustrated in Figures 6a and 6d, respectively. Meanwhile, Figures 6b and 6e show plots of the estimated T and S distributions using

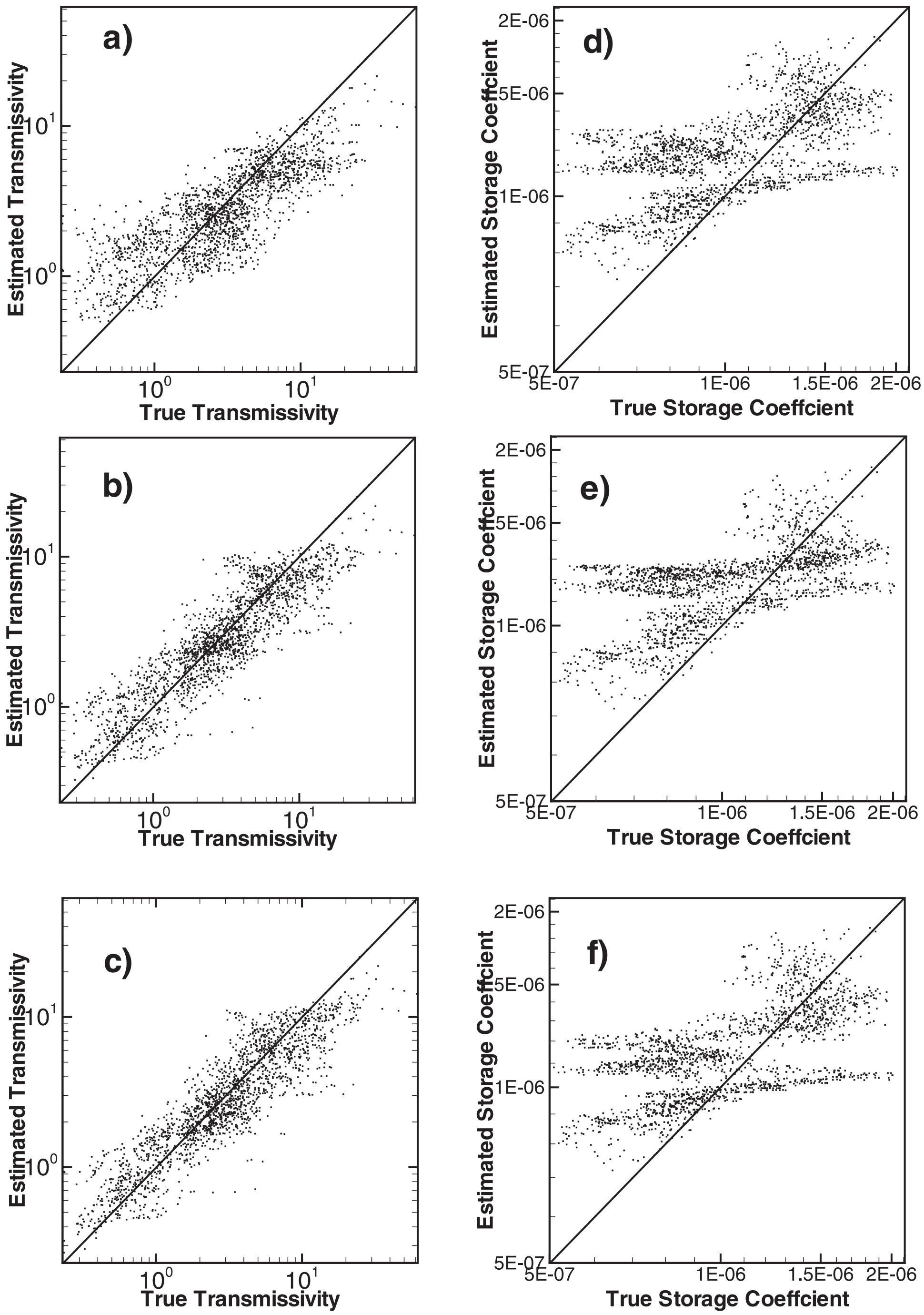

Figure 7. Scatterplots of true versus estimated values of the transmissivity and storage coefficients for the three cases.

the head changes at times 30,000 and 60,000 s (case 2). The estimated T and S distributions based on the head changes at times 30,000, 60,000 and 90,000 s (case 3) are shown in Figures 6c and 6f, respectively. Note that for each case, the inverse modeling commenced at time 0.0 s. For cases 1–3, the iterative procedure in the SimSLE was terminated at 13th, 15th, and 16th iterations, respectively, on the basis of the relative change in the conditional L2 measure (equation (13)).

[39] Scatterplots of estimated versus true T fields for the three cases are shown in Figures 7a–7c and the corresponding plots for S are presented in Figures 7d–7f. Performance metrics of the estimates for the three cases are summarized in Table 1. The final estimated T field corroborates very well with the true field (correlation = 0.901) while the estimated S field only attains a correlation of 0.613 with the true S field.

[40] According to Figures 6 and 7 and the performance metrics in Table 1, the estimate of the T field improves as groundwater level data at different times, corresponding to different locations of the river disturbance during its downstream migration, are included in the inversion. The improvement of the estimated S field however is not obvious.

Table 1. Statistical Measures for Comparison of the Estimated Parameters and Their True Fields[a]

	Transmissivity				Storage Coefficient			
	L1	L2	Cor	Sim	L1	L2	Cor	Sim
Case 1	0.465	0.350	0.818	0.782	0.228	0.0836	0.606	0.628
Case 2	0.349	0.205	0.894	0.845	0.233	0.0864	0.587	0.621
Case 3	0.335	0.192	0.901	0.854	0.217	0.0751	0.613	0.642
Case 4, noise free	0.399	0.261	0.861	0.827				
Case 4 with noise	0.462	0.358	0.801	0.801				

[a]Cor is correlation, and Sim is simulation.

[41] Distribution of the residual variances (uncertainty) of the estimated T for cases 1, 2, and 3 are shown in Figures 8a, 8b, and 8c, respectively. These figures show that the residual variances generally increase as the distance from the river or the excitation source increases. On the other hand, residual variance of the storage coefficient (Figures 8d, 8e, and 8f) is generally seen to depend on the distance between location of the river disturbance and observation well. That is, the shorter the distance between the well and flood disturbance, the smaller the uncertainty of the estimate, and the longer the distance, the larger the uncertainty of the estimate.

[42] Finally, in case 4, the observed initial, steady groundwater levels with and without noise were used to estimate the T field. Notice that this case uses only a single "snapshot" of the aquifer heterogeneity and thus the river stage tomography concept is not involved. For this case, the iteration was stopped at 32nd iteration for the scenario using noise-free hydrographs and at 50th iteration for the case with noise infested hydrographs.

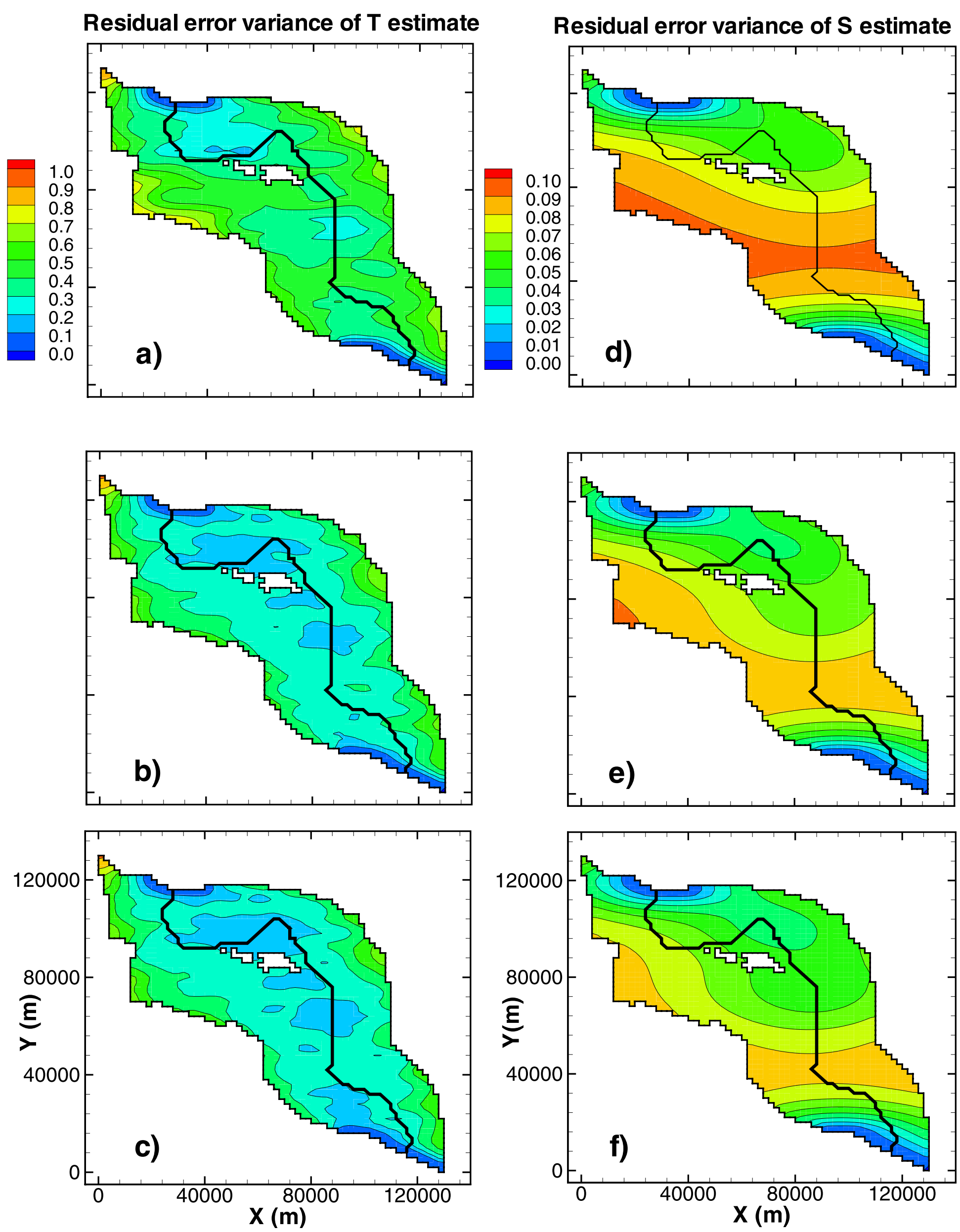

Figure 8. Residual error variance (uncertainty) of the estimated transmissivities for (a, b, c) cases 1, 2, and 3 and (d, e, f) the corresponding residual error variance of the storage estimates.

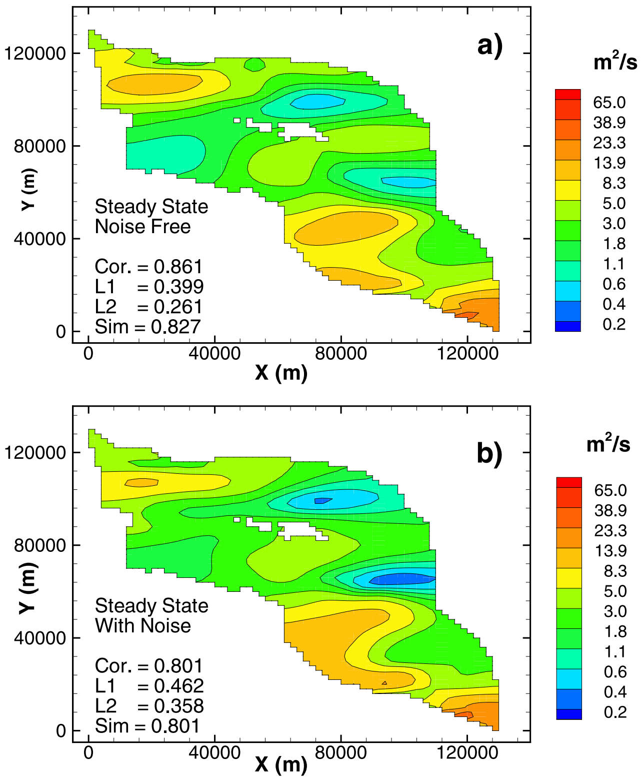

Figure 9. Estimated transmissivity field (a) using noise-free initial steady state groundwater level data and (b) using the data with noise.

[43] Figure 9a illustrates the estimated T field on the basis of 36 noise-free well hydrographs, corresponding to the initial steady streamflow, whereas Figure 9b shows the estimated field on the basis of the hydrographs with noise. The performance metrics are also presented in Figure 9. Scatterplots for the estimates using the noise free and with noise data are shown in Figures 10a and 10b, respectively. No estimate of S field is attempted since this case involves only steady flow. As expected, T estimates based on the 36 noise-free hydrographs are superior to those based on the noisy ones. Since they are initial head data, no wavelet denoising was attempted.

[44] In comparison with the T field estimated by the river stage tomography, most of the estimated T values using the steady state head information align more closely to the 45° line (unbiased), whereas some values disperse greater around the line. As a result, on the average, they are not as robust as those from the river stage tomography as reflected in the performance metrics. This comparison further vindicates the usefulness of the river stage tomography. That is, as the river stage perturbation migrates to one location along the river, it produces a head response in various parts of the aquifer. These responses constitute a snapshot of the heterogeneity of the aquifer with a hydraulic excitation source at the location of the disturbance. As the flood wave continuously migrates downstream and aquifer responses at various times are collected, we thereby have a large number of snapshots of the aquifer heterogeneity with sources at different locations. These snapshots provide us with the view of the aquifer heterogeneity at different angles and perspectives. Synthesizing these different views lead to a better characterization of the aquifer heterogeneity than using one snapshot.

[45] The cross-correlation analysis between the head at an observation well and heterogeneous T field in an aquifer during a pumping test by *Wu et al.* [2005] and *Zhu et al.* [2009] may shed light on the above finding. That is, the steady state (or late time) head perturbation at the observation well positively correlates at various degrees with T values over a large region within the cone of depression. The T estimates using the 36 initial groundwater levels during the steady streamflow are thus satisfactory. The estimation, however, does not take advantage of the river stage tomographic survey which provides additional nonredundant data sets to improve the estimate. *Wu et al.* [2005] and *Zhu et al.* [2009] also reported that the head perturbation is highly correlated with S values in a narrow strip between the pumping and observation wells only at early time. Head changes during the early time are known to be small and they are prone to noise (small signal-to-noise ratio). As a consequence, the river stage tomography is not effective for the estimation of the S field. *Xiang et al.* [2009]

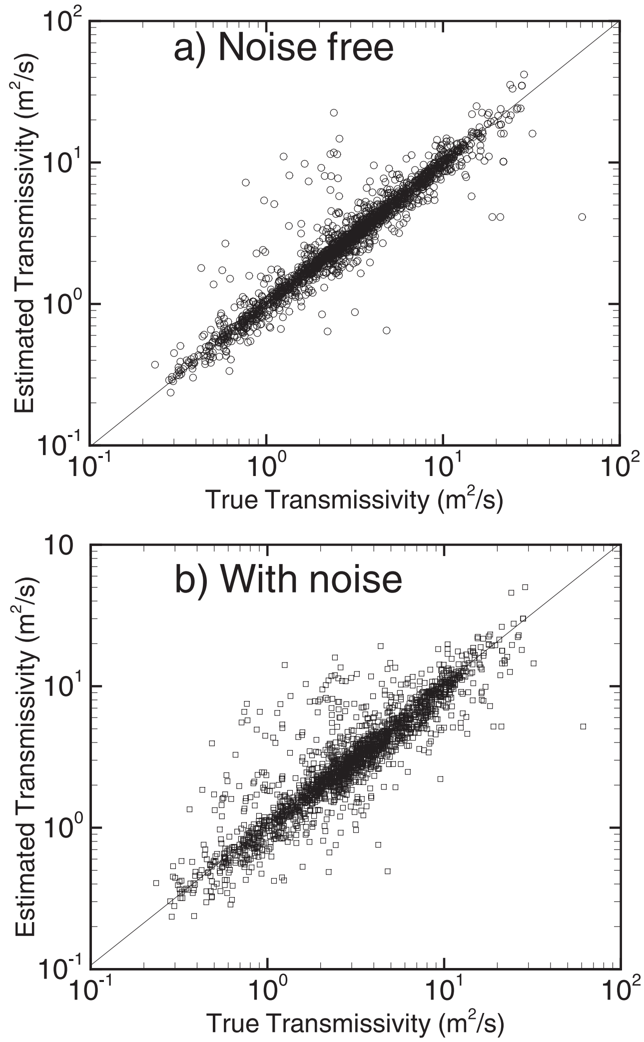

Figure 10. Scatterplots of the true transmissivity field and the estimates (a) using noise-free initial steady state groundwater level data and (b) using the data with noise.

offered a similar explanation for the difficulty in estimating the S field using well hydraulic tomography.

5. Discussion

[46] This study has demonstrated that the river stage hydraulic tomography provides useful information for delineating basin-scale aquifer heterogeneity; our estimation algorithm is effective for the synthetic case: a proof of concept. Their applications to real-world situations, nevertheless, deserve further investigations. In real-world situations, well hydrographs undoubtedly are influenced by many excitations such as earth tides, barometric pressure variations, precipitation, evapotranspiration, recharge, groundwater withdrawal, in addition to river stage variations. Influences of these excitations should bear their own signatures and characteristics (i.e., frequencies and amplitudes). Therefore, signals from different excitations can be separated if the excitation characteristics are known and they are not identical. Otherwise, a wavelet denoising procedure may be used as demonstrated in this study, perhaps at the expense of the final resolution of heterogeneity since wavelet denoising may remove signals of heterogeneity. In spite of these difficulties, we believe that groundwater water level fluctuations induced by the spatial/temporal river stage variations can be used to estimate aquifer heterogeneity as a large-scale hydraulic tomographic survey as long as the signal-to-noise ratio is sufficiently high.

[47] The signal-to-noise ratio depends on the strength of the groundwater level change induced by the change in river stage (signal) and of those caused by other phenomena (noise). The strength of the signal is controlled by the magnitude of changes in the river stage, the aquifer hydraulic characteristics (i.e., hydraulic conductivity, specific storage or diffusivity), and the type of interaction between the river and the aquifer as well as confined or unconfined characteristics of the aquifer. For example, the characteristic behavior of perennial rivers connected with the aquifer (stream fully/partially penetrating an unconfined/confined aquifer) during the propagation of a flood wave in the river can be described as recharge to the aquifer initially and then discharge to the river when the flood wave recedes [see *Sophocleous*, 2002; *Winter et al.*, 1998]. In such systems, the net flood-induced recharge may be small, but the pressure pulses which form the basis for river stage tomography can rapidly propagate over large distances particularly in confined aquifers as observed by *Sophocleous* [1991]. The distance from the river where pressure changes can be detected will certainly depend on sensor accuracy.

[48] On the other hand, SWGW systems in areas of low precipitation are characterized by unconfined aquifers underlying ephemeral streams. The stream and the aquifer may be considered as connected only partially via a variably saturated zone which may consist of a large amount of air. During floods, however, the strength of the signal induced by the change in the river stage is likely to be damped out over a short distance because of the presence of air. In these cases, the effectiveness of the river stage tomography may be limited to the vicinity of the river. Nevertheless, no aquifer is perfectly confined or unconfined in a groundwater basin. In summary, the effectiveness of river stage tomography may be site and event-dependent.

[49] Our attempt to apply a similar approach to groundwater basins in Taiwan [*Yeh et al.*, 2004] has revealed that most well hydrographs have been sampled on an hourly basis or even longer intervals. The aquifer response to rapid flood migration due to the steep profiles of rivers in Taiwan was not monitored effectively. Further controlled large-scale field investigations are clearly needed to understand the relation between river stages and aquifer responses and extent of propagation of the excitation at various river basins. Perhaps, more accurate and frequent sampling of river stage variations and well hydrographs is required in order to capture these signals. Certainly, careful numerical experiments using a realistic 3-D integrated surface and groundwater model (e.g., HydroGeoSphere [*Therrien et al.*, 2006]) may provide guides to design such monitoring networks and experiments.

6. Conclusions

[50] We have presented a basin-scale aquifer characterization approach based on the concept of recently developed well hydraulic tomography. The aquifer characterization approach takes advantage of natural stimuli such as changes in river stages (migration of the river flow disturbance) to estimate the aquifer properties over a groundwater basin or aquifers along the river in a basin. We have demonstrated using a numerical example that the relation between a moving flood wave (source of excitation, perhaps, seasonal variations in river stage at different reaches of a river basin) and continuous well hydrographs indeed provide useful information for delineating basin-scale aquifer heterogeneity. While actual applications of this concept and technology to field problems remain to be explored further, the result of this study may facilitate better hydrologic observation strategies to characterize our subsurface environments in the future.

[51] **Acknowledgments.** The first author would like to acknowledge support from the National Cheng-Kung University during his visits in 2006, 2007, and 2008. Support from the Strategic Environmental Research and Development Program (SERDP) subcontracted through the University of Iowa as well as funding from the National Science Foundation (NSF) through grants EAR-0229717, IIS-0431079, and EAR-0450388 are acknowledged. We thank Andrew J. Guswa and three anonymous reviewers for constructive and insightful suggestions and Resta Cheng for the editing.

References

Barlebo, H. C., M. C. Hill, and D. Rosbjerg (2004), Investigating the Macrodispersion Experiment (MADE) site in Columbus, Mississippi, using a three-dimensional inverse flow and transport model, *Water Resour. Res.*, *40*, W04211, doi:10.1029/2002WR001935.

Barlow, P. M., L. A. DeSimone, and A. F. Moench (2000), Aquifer response to stream-stage and recharge variations. II. Convolution method and applications, *J. Hydrol.*, *230*(3–4), 211–229, doi:10.1016/S0022-1694(00)00176-1.

Bohling, G. C., X. Zhan, J. J. Butler Jr., and L. Zheng (2002), Steady shape analysis of tomographic pumping tests for characterization of aquifer heterogeneities, *Water Resour. Res.*, *38*(12), 1324, doi:10.1029/2001WR001176.

Bohling, G. C., J. J. Butler Jr., X. Zhan, and M. D. Knoll (2007), A field assessment of the value of steady shape hydraulic tomography for characterization of aquifer heterogeneities, *Water Resour. Res.*, *43*, W05430, doi:10.1029/2006WR004932.

Brauchler, R., R. Liedl, and P. Dietrich (2003), A travel time based hydraulic tomographic approach, *Water Resour. Res.*, *39*(12), 1370, doi:10.1029/2003WR002262.

Bredehoeft, J. D. (2003), From models to performance assessment: The conceptualization problem, *Ground Water*, *41*(5), 571–577, doi:10.1111/j.1745-6584.2003.tb02395.x.

Chen, X., and X. Chen (2003), Stream water infiltration, bank storage, and storage zone changes due to stream-stage fluctuations, *J. Hydrol.*, *280*(1–4), 246–264, doi:10.1016/S0022-1694(03)00232-4.

Davis, E. E., K. Wang, K. Becker, and R. E. Thomson (2000), Formation-scale hydraulic and mechanical properties of oceanic crust inferred from pore pressure response to periodic seafloor loading, *J. Geophys. Res.*, *105*(B6), 13,423–13,435, doi:10.1029/2000JB900084.

Desmarais, K., and S. Rojstaczer (2002), Inferring groundwater flow paths from measurements of carbonate spring response to storms, *J. Hydrol.*, *260*(1), 118–134.

DeWiest, R. J. M. (1965), *Geohydrology*, 366 pp., John Wiley, New York.

Doherty, J. (2007), *PEST: Model-Independent Parameter Estimation User Manual*, 5th ed., Watermark Numer. Comput., Brisbane, Queensland, Australia.

Domenico, P. A., and F. W. Schwartz (1997), *Physical and Chemical Hydrogeology*, 506 pp., John Wiley, New York.

Duffy, C. J., L. W. Gelhar, and G. W. Gross (1978), Recharge and groundwater conditions in the western region of the Roswell Basin, *Rep. 100*, N. M. Water Resour. Res. Inst., Las Cruces, N. M.

Glover, K. C. (1988), A finite-element model for simulating hydraulic interchange of surface and ground water, *U. S. Geol. Surv. Water Resour. Invest. Rep., 86-4319*, 90 pp.

Gottlieb, J., and P. Dietrich (1995), Identification of the permeability distribution in soil by hydraulic tomography, *Inverse Probl.*, *11*, 353–360, doi:10.1088/0266-5611/11/2/005.

Gutjahr, A. (1989), Fast Fourier transforms for random field generation, *N. M. Tech. Proj. Rep. Contract 4-R58-2690 R, N*, N.M. Inst. of Min. and Technol., Socorro, N. M.

Hagen, A. (2003), Fuzzy set approach to assessing similarity of categorical maps, *Int. J. Geogr. Inf. Sci.*, *17*(3), 235–249, doi:10.1080/13658810210157822.

Hao, Y., T.-C. J. Yeh, J. Xiang, W. A. Illman, K. Ando, and K.-C. Hsu (2008), Hydraulic tomography for detecting fracture connectivity, *Ground Water*, *46*(2), 183–192, doi:10.1111/j.1745-6584.2007.00388.x.

Henderson, F. M. (1989), *Open Channel Flow*, 522 pp., MacMillan, New York.

Hsieh, P. A., J. D. Bredehoeft, and S. A. Rojstaczer (1988), Response of well aquifer systems to Earth tides: Problem revisited, *Water Resour. Res.*, *24*(3), 468–472, doi:10.1029/WR024i003p00468.

Illman, W. A., X. Liu, and A. Craig (2007), Steady-state hydraulic tomography in a laboratory aquifer with deterministic heterogeneity: Multi-method and multiscale validation of K tomograms, *J. Hydrol.*, *341*(3–4), 222–234, doi:10.1016/j.jhydrol.2007.05.011.

Illman, W. A., X. Liu, S. Takeuchi, T.-C. J. Yeh, K. Ando, and H. Saegusa (2009), Hydraulic tomography in fractured granite: Mizunami Underground Research site, Japan, *Water Resour. Res.*, *45*, W01406, doi:10.1029/2007WR006715.

Kimbrough, R. K., G. P. Ruppert, W. D. Wiggins, R. R. Smith, and D. L. Kresch (2006), Water resources data—Washington water year 2005, *U. S. Geol. Surv. Water Data Rep., WA-05-1*.

Kollet, S. J., and V. A. Zlotnik (2003), Stream depletion predictions using pumping test data from a heterogeneous stream-aquifer system (a case study from the Great Plains, USA), *J. Hydrol.*, *281*(1–2), 96–114, doi:10.1016/S0022-1694(03)00203-8.

Konikow, L. F., and J. D. Bredehoeft (1992), Ground-water models cannot be validated, *Adv. Water Resour.*, *15*, 75–83, doi:10.1016/0309-1708(92)90033-X.

Kuhlman, K. L., A. C. Hinnell, P. K. Mishra, and T.-C. J. Yeh (2008), Basin-scale transmissivity and storativity estimation using hydraulic tomography, *Ground Water*, *46*(5), 706–715, doi:10.1111/j.1745-6584.2008.00455.x.

Kümpel, H. J., G. Grecksch, K. Lehmann, D. Rebscher, and K. C. Schulze (1999), Studies of in situ pore pressure fluctuations at various scales, *Oil Gas Sci. Technol.*, *54*(6), 679–688.

Li, W., A. Englert, O. A. Cirpka, J. Vanderborght, and H. Vereecken (2007a), Two-dimensional characterization of hydraulic heterogeneity by multiple pumping tests, *Water Resour. Res.*, *43*, W04433, doi:10.1029/2006WR005333.

Li, H., G. Li, J. Cheng, and M. C. Boufadel (2007b), Tide-induced head fluctuations in a confined aquifer with sediment covering its outlet at the sea floor, *Water Resour. Res.*, *43*, W03404, doi:10.1029/2005WR004724.

Liu, S., T.-C. J. Yeh, and R. Gardiner (2002), Effectiveness of hydraulic tomography: Sandbox experiments, *Water Resour. Res.*, *38*(4), 1034, doi:10.1029/2001WR000338.

Liu, X., W. A. Illman, A. J. Craig, J. Zhu, and T.-C. J. Yeh (2007), Laboratory sandbox validation of transient hydraulic tomography, *Water Resour. Res.*, *43*, W05404, doi:10.1029/2006WR005144.

Mallat, S. (1999), *A Wavelet Tour of Signal Processing*, 577 pp., Academic, San Diego, Calif.

Moench, A. F., and P. M. Barlow (2000), Aquifer response to stream-stage and recharge variations. I. Analytical step-response functions, *J. Hydrol.*, *230*(3–4), 192–210, doi:10.1016/S0022-1694(00)00175-X.

Nevulis, R. H., D. R. Davis, and S. Sorooshian (1989), Analysis of natural groundwater level variations for hydrogeologic conceptualization, Hanford site, Washington, *Water Resour. Res.*, *25*(7), 1519–1529, doi:10.1029/WR025i007p01519.

Poeter, E. P., M. C. Hill, E. R. Banta, S. Mehl, and S. Christensen (2005), UCODE_2005 and six other computer codes for universal sensitivity analysis, calibration, and uncertainty evaluation, in *U. S. Geol. Surv. Techniques Methods, 6-A11*.

Rojstaczer, S. (1988), Determination of fluid flow properties from the response of water levels in wells to atmospheric loading, *Water Resour. Res.*, *24*(11), 1927–1938, doi:10.1029/WR024i011p01927.

Rojstaczer, S., and F. S. Riley (1990), Response of the water level in a well to Earth tides and atmospheric loading under unconfined conditions, *Water Resour. Res.*, *26*(8), 1803–1817.

Rotting, T., J. Carrera, J. Bolzicco, and J. M. Salvany (2006), Stream-stage response tests and their joint interpretation with pumping tests, *Ground Water*, *44*(3), 371–385, doi:10.1111/j.1745-6584.2005.00138.x.

Sophocleous, M. A. (1991), Stream-floodwave propagation through the Great Bend alluvial aquifer, Kansas: Field measurements and numerical simulations, *J. Hydrol.*, *124*, 207–228, doi:10.1016/0022-1694(91)90015-A.

Sophocleous, M. A. (2002), Interactions between groundwater and surface water: The state of the science, *Hydrogeol. J.*, *10*, 52–67, doi:10.1007/s10040-001-0170-8.

Sophocleous, M., W. E. Bardsley, and J. Healey (2006), A rainfall loading response recorded at 300 m depth: Implications for geological weighing lysimeters, *J. Hydrol.*, *319*, 237–244, doi:10.1016/j.jhydrol. 2005.06.031.

Straface, S., T.-C. J. Yeh, J. Zhu, S. Troisi, and C. H. Lee (2007), Sequential aquifer tests at a well field, Montalto Uffugo Scalo, Italy, *Water Resour. Res.*, *43*, W07432, doi:10.1029/2006WR005287.

Therrien, R., R. McLaren, E. A. Sudicky, and S. Panday (2006), HydroGeo-Sphere, a three-dimensional numerical model describing fully integrated subsurface and surface flow and solute transport, Groundwater Simul. Group, Waterloo, Ont., Canada.

Thorne, P. D., M. P. Bergeron, M. D. Williams, and V. L. Freedman (2006), Groundwater data package for Hanford assessments, *PNNL-14753*, rev. 1, Pac. Northwest Natl. Lab., Richland, Wash.

Trescott, P. C., G. F. Pinder, and S. P. Larson (1976), Finite-difference model for aquifer simulation in two dimensions with results of numerical experiments, *U. S. Geol. Surv. Tech. Water Resour. Invest.*, *Book 7, Chap. C1*, 116 pp.

Vasco, D. W., H. Keers, and K. Karasaki (2000), Estimation of reservoir properties using transient pressure data: An asymptotic approach, *Water Resour. Res.*, *36*(12), 3447–3465, doi:10.1029/2000WR900179.

Vazquez-Sune, E., B. Capino, E. Abarca, and J. Carrera (2007), Estimation of recharge from floods in disconnected stream-aquifer systems, *Ground Water*, *45*(5), 579–589, doi:10.1111/j.1745-6584.2007.00326.x.

Vesselinov, V. V., S. P. Neuman, and W. A. Illman (2001), Three-dimensional numerical inversion of pneumatic cross-hole tests in unsaturated fractured tuff: 2. Equivalent parameters, high-resolution stochastic imaging and scale effects, *Water Resour. Res.*, *37*(12), 3019–3042, doi:10.1029/2000WR000135.

Winter, T. C. (1999), Relation of streams, lakes, and wetlands to groundwater flow systems, *Hydrogeol. J.*, *7*, 28–45, doi:10.1007/s100400050178.

Winter, T. C., J. W. Harvey, O. L. Franke, and W. M. Alley (1998), Groundwater and surface water—A single resource, *U. S. Geol. Surv. Circ., 1139*. (Available at http://pubs.usgs.gov/circ/circ1139)

Wu, C.-M., T.-C. J. Yeh, J. Zhu, T. H. Lee, N.-S. Hsu, C.-H. Chen, and A.-F. Sancho (2005), Traditional analysis of aquifer tests: Comparing apples to oranges?, *Water Resour. Res.*, *41*, W09402, doi:10.1029/2004WR003717.

Xiang, J. W., and T.-C. J. Yeh (2005), Numerical simulation of river stage/precipitation Tomography, *Eos Trans. AGU*, *86*(52), Fall Meet. Suppl, Abstract H41E-0463.

Xiang, J., T.-C. J. Yeh, C.-H. Lee, K.-C. Hsu, and J.-C. Wen (2009), A simultaneous successive linear estimator and a guide for hydraulic tomography analysis, *Water Resour. Res.*, *45*, W02432, doi:10.1029/2008WR007180.

Yeh, T.-C. J., and C. H. Lee (2007), Time to change the way we collect and analyze data for aquifer characterization, *Ground Water*, *45*(2), 116–118, doi:10.1111/j.1745-6584.2006.00292.x.

Yeh, T.-C. J., and S. Liu (2000), Hydraulic tomography: Development of a new aquifer test method, *Water Resour. Res.*, *36*(8), 2095–2105, doi:10.1029/2000WR900114.

Yeh, T.-C. J., and P. A. Mock (1996), Structured approach for calibrating steady-state ground-water flow models, *Ground Water*, *34*(3), 444–450, doi:10.1111/j.1745-6584.1996.tb02025.x.

Yeh, T.-C. J., M. Jin, and S. Hanna (1996), An iterative stochastic inverse method: Conditional effective transmissivity and hydraulic head fields, *Water Resour. Res.*, *32*(1), 85–92, doi:10.1029/95WR02869.

Yeh, T.-C. J., K. Hsu, C. Lee, J. Wen, and C. Ting (2004), On the possibility of using river-stage tomography to characterize the aquifer properties of the Choshuishi alluvial fan, Taiwan, *Eos Trans. AGU*, *85*(47), Fall Meet. Suppl, Abstract H11D-0329.

Yeh, T.-C. J., C. H. Lee, K.-C. Hsu, and Y.-C. Tan (2007), Fusion of active and passive hydrologic and geophysical tomographic surveys: The future of subsurface characterization, in *Data Integration in Subsurface Hydrology*, *Geophys. Monogr. Ser.*, vol. 171, edited by D. W. Hyndman, F. D. Day-Lewis, and K. Singha, pp. 109–120, AGU, Washington, D. C.

Yeh, T.-C. J., et al. (2008), A view toward the future of subsurface characterization: CAT scanning groundwater basins, *Water Resour. Res.*, *44*, W03301, doi:10.1029/2007WR006375.

Zhu, J., and T.-C. J. Yeh (2005), Characterization of aquifer heterogeneity using transient hydraulic tomography, *Water Resour. Res.*, *41*, W07028, doi:10.1029/2004WR003790.

Zhu, J., and T.-C. J. Yeh (2006), Analysis of hydraulic tomography using temporal moments of drawdown recovery data, *Water Resour. Res.*, *42*, W02403, doi:10.1029/2005WR004309.

Zhu, J., X. Cai, and T.-C. J. Yeh (2009), Analysis of tracer tomography using temporal moments of tracer breakthrough curves, *Adv. Water Resour.*, *32*, 391–400.

Zlotnik, V. A., and H. Huang (1999), Effect of shallow penetration and streambed sediments on aquifer response to stream stage fluctuations (analytical model), *Ground Water*, *37*(4), 599–605, doi:10.1111/j.1745-6584.1999.tb01147.x.

K.-C. Hsu and C.-H. Lee (corresponding author), Department of Resources Engineering, National Cheng Kung University, Number 1 Ta-Hsueh Road, Tainan, 701, Taiwan. (leech@mail.ncku.edu.tw)

R. M. Suribhatla, J. Xiang, and T.-C. J. Yeh, Department of Hydrology and Water Resources, University of Arizona, 1133 East James E. Rodgers Way, Tucson, AZ 85721, USA.

J.-C. Wen, Department of Environmental and Safety Engineering, Research Center for Soil and Water Resources and Natural Disaster Prevention, National Yunlin University of Science and Technology, Touliu, Yunlin, 64045, Taiwan.